Article

Structural Basis for the Inhibition of Gas Hydrates by α-Helical Antifreeze Proteins

Tianjun Sun,[1] Peter L. Davies,[1,2] and Virginia K. Walker[1,2,*]
[1]Department of Biomedical and Molecular Sciences and [2]Department of Biology, Queen's University, Kingston, Ontario, Canada

ABSTRACT Kinetic hydrate inhibitors (KHIs) are used commercially to inhibit gas hydrate formation and growth in pipelines. However, improvement of these polymers has been constrained by the lack of verified molecular models. Since antifreeze proteins (AFPs) act as KHIs, we have used their solved x-ray crystallographic structures in molecular modeling to explore gas hydrate inhibition. The internal clathrate water network of the fish AFP Maxi, which extends to the protein's outer surface, is remarkably similar to the {100} planes of structure type II (sII) gas hydrate. The crystal structure of this water web has facilitated the construction of in silico models for Maxi and type I AFP binding to sII hydrates. Here, we have substantiated our models with experimental evidence of Maxi binding to the tetrahydrofuran sII model hydrate. Both in silico and experimental evidence support the absorbance-inhibition mechanism proposed for KHI binding to gas hydrates. Based on the Maxi crystal structure we suggest that the inhibitor adsorbs to the gas hydrate lattice through the same anchored clathrate water mechanism used to bind ice. These results will facilitate the rational design of a next generation of effective green KHIs for the petroleum industry to ensure safe and efficient hydrocarbon flow.

INTRODUCTION

Gas hydrates are ice-like clathrate structures composed of water cages surrounding trapped gas molecules, which, depending on the gas, can form at temperatures above 0°C and at modest pressures (0.5 to several MPa) (1). In nature, they most commonly exist in two distinct forms, cubic structures I and II (sI and sII). These consist of a combination of small 12-faced pentagonal dodecahedron cages (5^{12}) and other water cages. For sII, there are 16 small cages and eight $5^{12}6^4$ large cages per unit cell (Fig. 1 *A*). Small guest molecules such as methane tend to promote sI formation, whereas larger gas molecules like propane promote sII crystals (2). Although gas hydrate deposits are a potential energy source, the unscheduled formation of gas hydrates is a major problem for the petroleum industry, since they can cause blockages at well heads and inside pipelines, with potentially disastrous consequences (3).

There are two major classes of inhibitors used for controlling hydrate formation and growth. Thermodynamic inhibitors, such as methanol, shift the equilibrium for hydrate formation (4), but due to their high cost, safety concerns, and potential to catalyze hydrate formation (5), there has been a move toward the application of kinetic hydrate inhibitors (KHIs). Unlike thermodynamic inhibitors, KHIs can delay hydrate nucleation and/or interfere with the crystal growth (6,7). Typically, these are water-soluble polymers that are effective at low concentrations. KHIs likely act by an adsorption-inhibition mechanism similar to the action of antifreeze protein (AFP) inhibition of ice growth. Indeed, AFPs can inhibit gas hydrate propagation, notwithstanding the distinct differences in the crystal structures of hydrates and ice. These have been dubbed green hydrate inhibitors and their potential for commercial use is in an explorative phase.

AFPs are produced by many organisms, such as the winter flounder that live in icy, subzero environments. This flatfish inhabits cold, shallow waters of the North West Atlantic. During the winter, the flounder secretes two distinct isoforms of an AFP into the blood. Type I AFP is a small (3 kDa) alanine-rich, α-helical monomer with an 11-residue periodicity, whereas the larger isoform, referred to as Maxi, is five times as long as the type I AFP and forms a 33-kDa homodimer (8,9). As with AFPs from other organisms, both forms bind to ice through a flat and relatively hydrophobic ice-binding surface (IBS). For at least one AFP, there is crystallographic evidence that waters associated with the protein are organized into a quasi-liquid/ice layer (10–13). These ice-like waters may facilitate the binding of AFP to ice by a mechanism termed the anchored clathrate water (ACW) hypothesis (14).

The x-ray crystal structure of Maxi shows that both 290-Å-long helix monomers fold in the middle through 180° (Fig. 1 *B*) (15). In the dimer, the two hairpins are packed so that both N-terminal helices lie adjacent to each other in an antiparallel orientation, as do the two C-terminal helices. The resulting four-helical bundle retains ~400 clathrate waters in the core (16). The internal waters are organized into two intersecting polypentagonal networks (Fig. 1 *C*). An intrachain water sheet lies between the N-terminal

Submitted May 28, 2015, and accepted for publication August 31, 2015.

*Correspondence: walkervk@queensu.ca

Editor: Nathan Baker.

0006-3495/15/10/1698/8

http://dx.doi.org/10.1016/j.bpj.2015.08.041

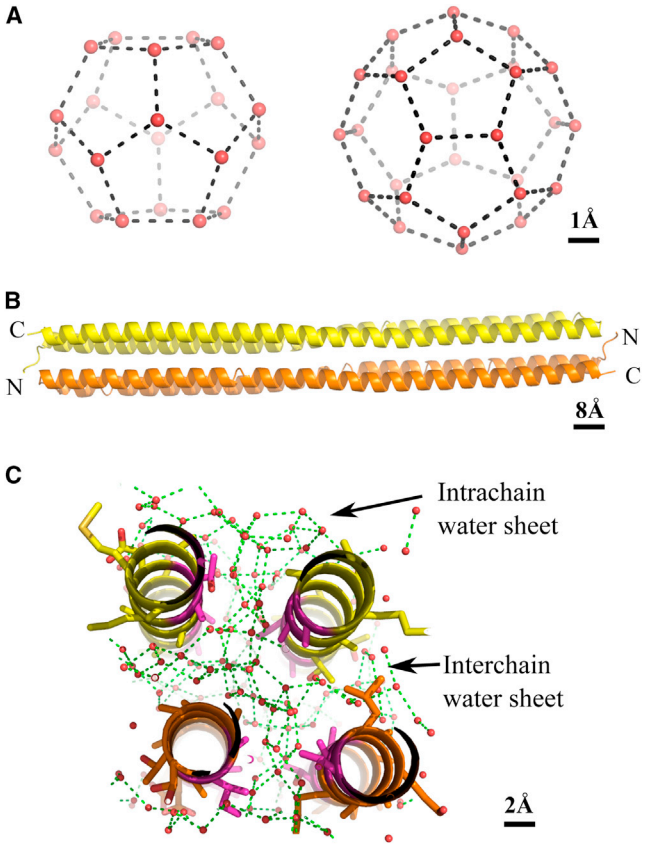

FIGURE 1 Overview of sII gas hydrate and Maxi structures. (*A*) Small and large sII gas hydrate water cages with waters (*red spheres*) and their hydrogen bonds (*dashed lines*) indicated. (*B*) Crystal structure of Maxi. The two antiparallel monomers are colored yellow and orange, with the N- and C-terminal ends as indicated. (*C*) Cross section of Maxi. The intra- and interchain water sheets are shown with waters (*red spheres*) and their hydrogen bonds (*dashed lines*). The side chains of Maxi are shown as sticks, with the ice-binding residues colored purple. To see this figure in color, go online.

arms and C-terminal arms, whereas an interchain water web is sandwiched between the two monomers. The ice-binding residues of type I AFP (i Thr, i+4 Ala, i+8 Ala) are also conserved in the Maxi sequence, but in this larger isoform, they point inward to bind and coordinate the intrachain water network (Fig. 1 *C*). The interior residues at the dimer interface interact with the interchain water monolayer. These interactions, which are primarily hydrogen bonds and van der Waals interactions, likely stabilize the folding of the protein and probably substitute for protein contacts between the helices. In Maxi, the ordered waters extend outward from the protein surface and are thought to be involved in ice binding.

In contrast to our growing understanding of the adsorption of AFPs to ice, the binding of KHIs to hydrates is more challenging to elucidate due to a lack of solved inhibitor-gas hydrate complex structures. Some in silico models have been made both with molecular dynamics (MD) and Monte Carlo simulations, but the lack of detailed information on KHIs has also made the use of these algorithms problematic (3). This is unfortunate, since it hinders the rational design of more effective hydrate inhibitors for the petroleum industry. Here, we have taken, to our knowledge, a novel approach to this problem. Since AFPs inhibit hydrate formation as effectively as some commercially used KHIs (17–19), and based on the striking match of internal clathrate waters of Maxi to sII gas hydrate structures, we have now modeled the adsorption of Maxi and the simpler type I AFP with the {100} planes of the sII gas hydrate.

MATERIALS AND METHODS

Modeling

In silico models were built using PyMOL 1.54 (20). To assemble the model of Maxi binding to sII hydrate, the edges of the hydrate-like region (HLR) were merged with the {100} plane by superimposing the HLR on the hydrate plane. A model for type I AFP binding to sII hydrate was obtained by first superimposing type I AFP on the helical arms of Maxi including the HLR of the associated waters. Subsequently, the gas hydrate {100} plane was matched to the HLR.

MD simulation of type I AFP

Simulations with type I AFP used coordinates obtained from the Protein Data Bank (PDB: 1WFB) and were performed using the program Gromacs v. 4.6.1 (21) and the TIP4P water model. The protein was solvated in a rectangular box (71.6 × 39.7 × 49.6 Å) containing 4521 water molecules. After energy minimization, a 400-ps position-restrained MD simulation was performed to relax the solvent around the protein at −0.15°C. The Charmm27 force field was used, along with Berendsen temperature and pressure coupling. A full-scale 20-ns MD simulation was then performed.

To calculate the water density around each of the protein models, the coordinates from the MD simulations were aligned by least-squares fit of the protein backbone using the first frame as a reference. Water density was calculated using the VolMap plugin (version 1.1) of VMD (version 1.9.1) with a resolution of 0.5 Å, atom size of 1 Å, weights as mass, and computed as the average for all saved frames. The calculation was performed on a cluster of high-speed computers at the High Performance Computing Virtual Laboratory accessed through Queen's University.

Tetrahydrofuran hydrate binding

Recombinant Maxi was purified by three rounds of ammonium sulfate precipitation as described previously (15). Recombinant type III AFP (Swiss-Prot Database: P19414) was prepared as indicated (22). Cytochrome *c* (12 kDa) was purchased from Sigma Aldrich (St. Louis, MO). Polyvinylpyrrolidone (PVP; average molecular mass, ~10 kDa) was purchased from Sigma Aldrich. Proteins were fluorescently labeled with fluorescein isothiocyanate (FITC; Thermo Fisher Scientific, Waltham, MA) using the method described previously for tetramethylrhodamine labeling (23). It must be noted that because Maxi is more thermolabile than the other proteins used, care was taken to keep these protein solutions at <15°C.

Polycrystalline tetrahydrofuran (THF) clathrate hydrates were grown as previously described (19). Briefly, THF/water solutions (1:3.34, v/v; 80 mL) containing 4 μM protein (Maxi, type III AFP, or cytochrome *c*, or their FITC-labeled forms) or PVP were placed in a beaker at 4°C and the temperature of a hollow brass finger was slowly lowered (0.5°C every 30 min) so that an ice-like hydrate hemisphere was formed. Routinely, the THF polycrystalline hydrate was grown until half the volume of the

starting solution had crystallized. Hemispheres were grown in triplicate for each protein as follows: those formed in the presence of nonlabeled proteins were done in duplicate, whereas those formed in the presence of labeled proteins were done once and visualized under ultraviolet (UV) light and photographed. Hemispheres formed in the presence of PVP were done in duplicate. After recovery of the nonlabeled protein and PVP hemispheres, the THF was evaporated in a fume hood and the melted liquid was 20-fold concentrated. Maxi and cytochrome *c* samples were concentrated at 4°C using Centricon filters (Millipore, Billerica, MA). Since type III AFP tended to stick to the Centricon membrane, these samples were lyophilized and subsequently dissolved in water, as were the PVP samples. Protein concentration was assayed using dye binding with bicinchoninic acid (BCA Protein Assay Kit, Pierce, Rockford, IL). PVP concentrations were measured using absorbance at 220 nm relative to a standard curve (24).

RESULTS

The similarity between the internal water network of Maxi and the sII {100} planes

The symmetrical cubic sII hydrate has identical {100} type planes: (100), (010), (001), ($\bar{1}$00), (0$\bar{1}$0), and (00$\bar{1}$). As indicated, pentagonal (5^{12}) rings surround larger circular rings (Fig. 2 *A*) giving rise to a repetitive pattern in the {100} plane, with the basic unit defined as a network of 16 water molecules. The intrachain water sheet in the Maxi repetitive region also consists of many pentagonal water rings, with the occasional tetragonal and hexagonal rings, as well as larger circular water rings (Fig. 2 *B*). Indeed, the water web highlighted in Fig. 2 *B* shows a pattern very like the basic unit of the sII {100} planes connecting along the horizontal. Even the spacing between the equivalent waters in both regions is close at 17.3 Å and 16.5 Å for the hydrate planes and the Maxi water network, respectively (see Fig. 2, *A* and *B*, *dotted lines*). Because of this similarity, the highlighted portion of the Maxi's internal water network was designated the hydrate-like region (HLR). When Maxi's HLR was overlain on the {100} planes of the modeled sII hydrate, most waters in the HLR were superimposable with an RMSD of 0.95 Å for 48 waters (Fig. 2 *C*). In addition, a few waters that were just outside of the HLR superimposed well with the hydrate planes.

Model for Maxi binding to sII gas hydrate

In Maxi, waters on the edge of the HLR extend outward beyond the helix gaps to form the anchored clathrate region that is thought to bind the AFP to ice (15). Thus, a model for Maxi binding to sII hydrate was constructed by merging the edges of the HLR and the (100) plane of the hydrate (Fig. 3 *A*). These two sets of organized waters were seamlessly merged. Consequently, the top face of Maxi formed complementary interactions with the (001) plane of the gas hydrate (Fig. 3 *B*). In addition to the waters that extend from the Maxi protein core, waters anchoring to the carbonyl groups of the residues on the top surface of

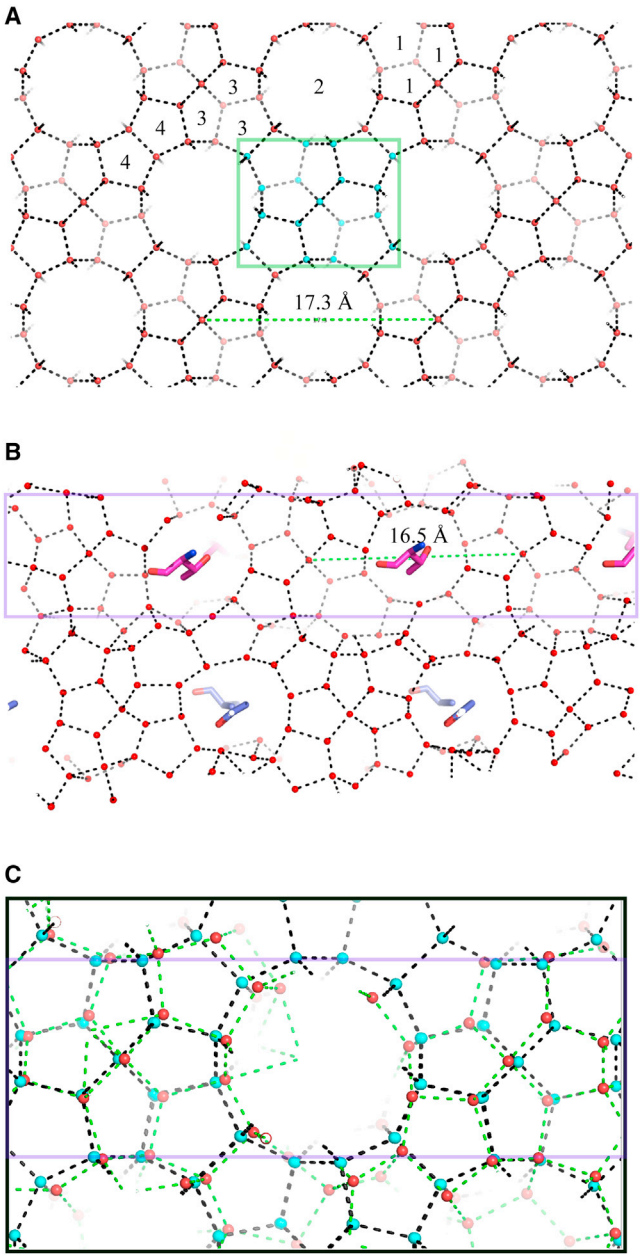

FIGURE 2 Similarity between the internal water network of Maxi and the {100} planes of sII gas hydrate. (*A*) Structure of {100} planes of type II gas hydrate with waters (*red spheres*) and hydrogen bonds (*black dashed lines*). Waters defining one repeating unit on the plane are colored in cyan and included in the green rectangle. The distance between the equivalent waters is shown. There are four types of grooves on the planes; one example for grooves 1, 2, 3, and 4 is shown such that the water rings forming them are labeled with the same number. (*B*) Intrachain water sheet of Maxi (side view). Notations are the same as in (*A*). Ice-binding residues of Maxi forming close contacts with each other are shown as sticks. The region highlighted by the purple square is similar to the plane of the gas hydrate. (*C*) Superimposition of a portion of HLR on the {100} planes of sII gas hydrate. Waters in the intrachain sheet (*red spheres*) and their hydrogen bonds (*green dashed lines*) are distinguished from hydrate waters (*cyan spheres*) and their hydrogen bonds (*black dashed lines*). The HLR is delineated by the purple lines. To see this figure in color, go online.

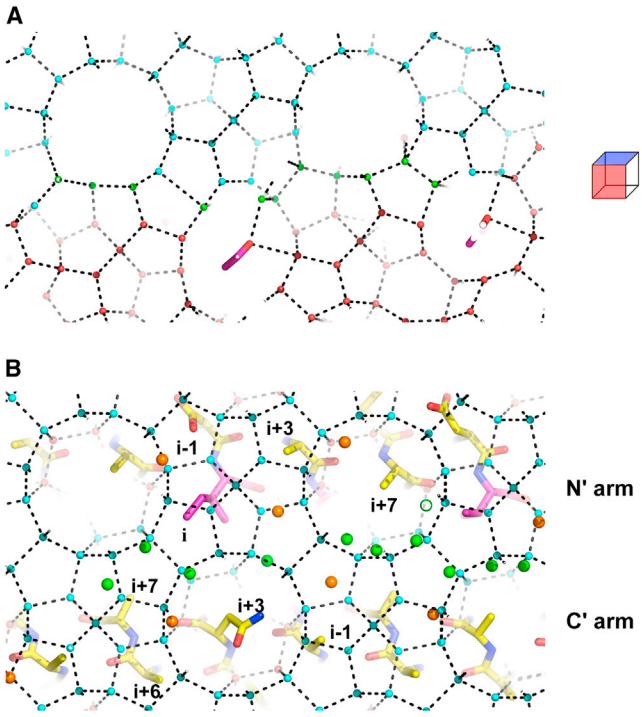

FIGURE 3 A model for Maxi binding to sII gas hydrate. (*A*) The edge of the HLR of Maxi merges seamlessly with the (100) plane of gas hydrate. Waters in HLR (*red spheres*) are differentiated from those at the edge of the HLR, which merge with the hydrate lattice (*green spheres*). Hydrate waters in the (100) plane (*cyan spheres*) and hydrogen bonds (*black dashed lines*) are indicated. Maxi is not shown except for a few ice-binding residues forming close contacts to each other. In the cube on the right, the (100) and (001) hydrate planes are shown in red and blue, respectively. (*B*) Top surface of Maxi forming complementary interactions with the (001) plane of the gas hydrate. Maxi is shown in stick representation with its carbon atoms (*yellow*), ice-binding residues (*purple*), and hydrate waters in the (001) plane (*cyan spheres*), and with their hydrogen bonds indicated (*black dashed lines*). Waters at the edge of the HLR (*green spheres*) and those anchoring to the top surface of Maxi (*orange spheres*) are shown. The periodic positions for residues that are accommodated in the hydrate groove are labeled. To see this figure in color, go online.

Maxi also matched well with waters on the hydrate (001) plane. In this configuration, the relative hydrophobic side chains on the protein surface fit well into the grooves of the hydrate plane. There are four types of grooves on the {100} planes of sII gas hydrate (Fig. 2 *A*). Side chains on the N-terminal arm (i, i+7, i+3, and i−1) docked into grooves 1, 2, 3, and 4, respectively. In addition, side chains on the C-terminal arm (i+7, i+3, i−1, and i+6) docked into the adjacent grooves 1, 2, 3, and 4, respectively. Three Asp residues (at i−1 positions along the N-terminal arm), have side-chain carbonyls that are capable of matching and thus substituting for waters in the plane. In this regard, it is notable that in an AFP from a bacterium (*Mp*AFP), Asp side chains on the ice-binding site mimic surface ice-like waters (14). This supports our contention that Maxi binds to the gas hydrate by merging the anchored surface waters to the hydrate plane.

Maxi experimentally adsorbs to THF hydrate

To demonstrate that Maxi was indeed capable of binding the sII hydrate, polycrystalline THF crystals were grown in the presence of Maxi or FITC-labeled Maxi. Parallel control experiments were performed with labeled type III AFP and cytochrome *c*, which served as positive and negative controls, respectively (17,19). THF hydrate polycrystals grown in solutions containing FITC-labeled Maxi and type III AFP emitted green light under UV illumination (Fig. 4, *A* and *B*). In contrast, the hydrate grown in the presence of FITC-labeled cytochrome *c* was uniformly dark under UV illumination (Fig. 4 *C*). The THF crystal grown in the Maxi solution was deeply etched compared to those grown with type III AFP and cytochrome *c* (Fig. 4, *D–F*), suggesting that Maxi interfered with the normal hydrate growth habit. To quantify adsorption, the hydrates were melted and assayed for protein. At a concentration of 4 μM protein in the starting THF solution, ~30% type III AFP was adsorbed and included in the polycrystalline hydrate, consistent with previous assessments (19). In contrast, ~50% of Maxi was adsorbed to the polycrystalline hydrate under the same conditions, whereas no cytochrome *c* was included in the gas hydrate (Fig. 5), demonstrating the exclusion of non-AFPs. At the same concentration and conditions, ~28% PVP was adsorbed to the polycrystalline hydrate (Fig. S1 in the Supporting Material), which is close to the value obtained with type III AFP but lower than the incorporation of Maxi.

Model for type I AFP binding to sII gas hydrate

Type I AFP, the small homolog of Maxi, has previously been shown to experimentally bind and inhibit hydrate growth

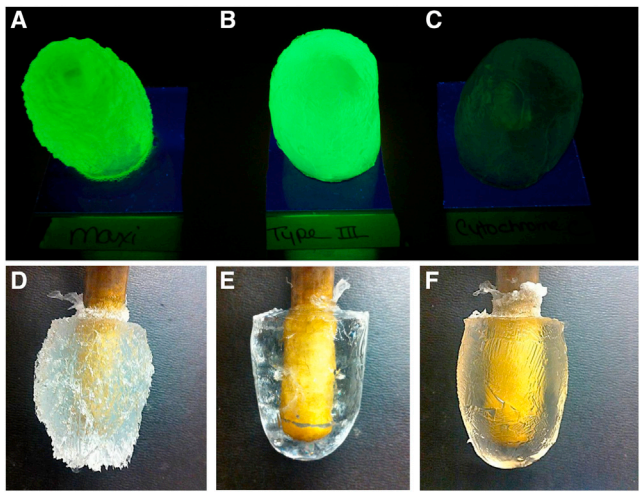

FIGURE 4 Polycrystalline THF crystals adsorb AFPs. (*A–C*) The hydrates grown in the presence of FITC-labeled Maxi (*A*), type III AFP (*B*), and cytochrome *c* (*C*), are illuminated with UV light. (*D–F*) THF hydrate fingers grown in solutions containing unlabeled Maxi (*D*), type III AFP (*E*), and cytochrome *c* (*F*). To see this figure in color, go online.

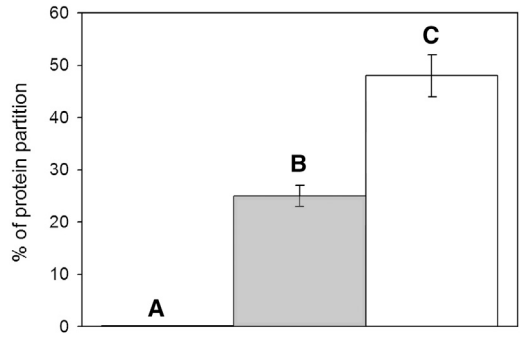

FIGURE 5 Partitioning of proteins into THF hydrate. The percentages of cytochrome *c* (*A*, *black*), type III AFP (*B*, *gray*), and Maxi (*C*, *white*) adsorbed into the hydrate are plotted as a bar graph. Measurements for each protein (4 μM) were done in duplicate. Bars indicate ranges.

(17). These two isoforms share key Thr and Ala residues that in Maxi point inward and form organizing interactions with the HLR of the internal water network (Fig. 1 *C*). In type I AFP, these residues are thought to have a more direct role in organizing the anchored clathrate waters that bind and fuse to ice (25). Therefore, we reasoned that a model for the binding of the smaller isoform to sII hydrate through the IBS could be built by superimposing type I AFP on the helical arms of Maxi including the HLR of the associated waters and subsequently matching it to the hydrate {100} planes. Since Maxi showed binding to the HLR through pairs of helical arms (N-terminal and C-terminal (Fig. 1 *C*)), two models were obtained.

Superimposition on the N-terminal helical arm of Maxi generated a model for type I AFP binding to sII gas hydrate that made intimate contacts, as shown in Fig. 6, *A* and *B* (*top* and *side views*, respectively). The side chains of the ice-binding residues (positions i (Thr), i+4 (Ala), and i+8 (Ala)) and a non-ice-binding residue (position i+1) docked into grooves 1, 2, 3, and 4, respectively. With surface waters on the hydrate-binding site of the AFP already preordered into a gas hydrate arrangement, AFP binding to the hydrate could occur from a simple merger of the preformed water layers. Hydrogen-bonding interactions also contributed to binding stability. As seen, the carbonyl groups of Maxi's ice-binding residues anchor to the HLR through hydrogen bonds. Also, the carbonyl groups of ice-binding residues (positions i+4 and i+8) formed hydrogen bonds with the gas hydrate {100} planes (Fig. 6 *B*).

When type I AFP was superimposed onto the C-terminal helical arm of Maxi, the resulting model for sII binding was equally snug (Fig. 6, *C* and *D*, *top* and *side views*, respectively). Here, the side chain of a non-ice-binding residue (position i+7), and the ice-binding residues (positions i, i+4, and i+8), docked into hydrate grooves 1, 2, 3, and 4, respectively (Fig. 6 *C*). Furthermore, the carbonyl groups of the ice-binding residues (positions i and i+4) formed hydrogen-bonding interactions with the gas hydrate (Fig. 6 *D*). In both of these N- and C-terminal models, two adjacent faces of type I AFP, rotated 33° from each other around the helix, were used to interact with grooves 1, 2, 3, and 4 on the {100} planes of the gas hydrate.

DISCUSSION

Maxi and type I AFPs adsorb to structure II gas hydrates

The impetus to model the interaction between type I AFP and the sII {100} planes was based on the crystal structure

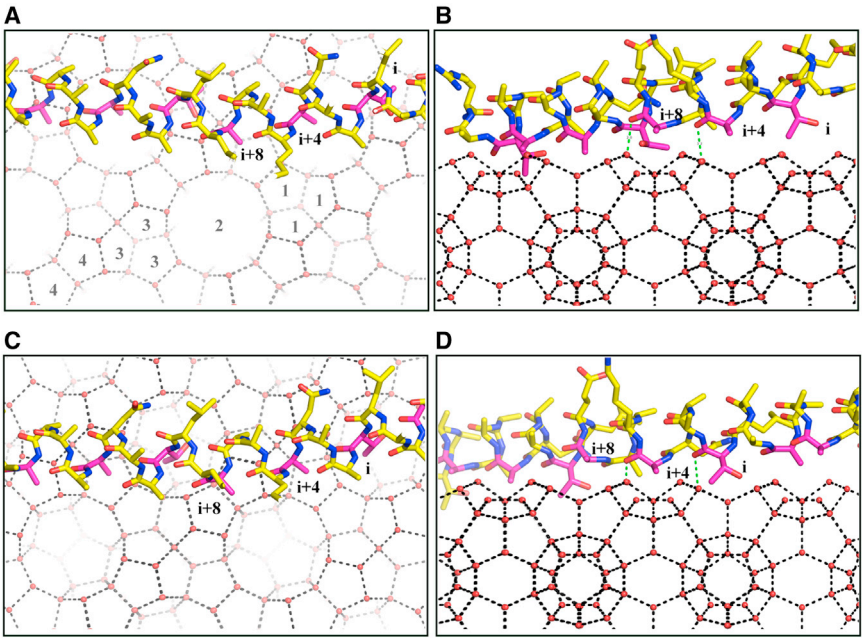

FIGURE 6 Models for type I AFP binding to the {100} planes of sII gas hydrate. Type I AFP (*stick representation*) with its carbon atoms (*yellow*) is shown with hydrate waters (*red spheres*) and their hydrogen bonds (*black dashed lines*). (*A*) Top view of the binding model where type I AFP is superimposed on the N-terminal helical arm of Maxi. One example for grooves 1, 2, 3, and 4 is shown such that the water rings forming them are labeled with the same number. The ice-binding residues (*purple*) are labeled, i, i+4, and i+8 at their periodic positions. (*B*) Side view of the binding model in (*A*). Hydrogen bonds (*green dashed lines*) between AFP and hydrate waters are shown. (*C*) Top down view of the binding model for type I AFP superimposed on the C-terminal helical arm of Maxi. (*D*) Side view of the binding model. To see this figure in color, go online.

of Maxi's internal waters, which make remarkable matches to those of gas hydrates (Fig. 2). Not surprisingly, since type I AFP and the sII {100} planes are similar to the helical arm and the HLR of Maxi, respectively, our proposed interactions are thermodynamically favorable. Further support of our model is afforded by previous experimental work showing that type I AFP inhibits THF hydrate growth (17). Based on the similarity between the HLR of Maxi and the sII {100} planes, we have also proposed a model of Maxi binding to hydrate, and this is supported by experimental evidence of Maxi's adsorption to polycrystalline THF hydrate (Figs. 4 and 5). Significantly more Maxi than type III AFP bound to the hydrate, consistent with our model that shows that Maxi binds to the hydrate through a large surface area. We further speculate that the observed morphological disruption of the polycrystalline hydrate surface is a result of this large surface binding.

Most KHIs are water-soluble polymers, with a common motif being an amide group with an adjacent hydrophobic group in the repeating unit. Two mechanisms have been suggested to explain their binding to gas hydrates, water perturbation and absorption-inhibition (26). The first mechanism posits that KHI functional groups perturb the water molecules at sufficient distances so that they are no longer available to join the crystal lattice. MD simulations with sI have shown some support for this hypothesis, at least for the commercially used KHI, PVP (27). However, a neutron diffraction study showed that the water structure in propane-water systems was not affected by PVP before and during gas hydrate formation (28). The second mechanism assumes that hydrophobic groups on the inhibitor polymers dock to cavities on the hydrate surface to mimic the small hydrocarbon guest molecules, whereas amide groups anchor to the surface through hydrogen bonding. The absorption mechanism was supported by studies on the growth inhibition of THF hydrate as well as by MD and Monte Carlo simulation studies (29–33).

Type I AFP and Maxi as biological KHIs are also polymers with 11-residue repeats. They also have backbone amide groups and hydrophobic side chains on their IBSs, similar to the common functional motifs of most KHIs. Preliminary MD simulations of type I AFP and sI methane surfaces gave some support for the absorption-inhibition hypothesis with adsorption driven by hydrophobic interactions and stabilized by hydrogen bonding (3). Here, however, we more compellingly show that the two AFPs with surface waters present are capable of directly adsorbing to sII gas hydrate. Hydrophobic side chains of the AFPs occupy cavities on the hydrate surface in the same way as the gas guest molecules. As shown in Fig. 3, the backbone carbonyl groups of Maxi anchor surface waters, which then merge with the water layer on the surface of the gas hydrate. This also holds true for type I AFP. A stable MD simulation of the latter AFP showed that the carbonyl groups of the ice-binding residues at positions i+4 and i+8 can anchor waters. When type I AFP docks according to the model in Fig. 6 *A*, these waters match with those on the {100} planes of hydrate (Fig. 7). Therefore, the crystal structure of Maxi and the MD simulation of type I AFP allow us to speculate about the hydrate binding process, where AFPs bind to the hydrate by simply merging the clathrate-like waters on their IBSs with the hydrate plane, analogous to the ACW water mechanism proposed for the binding of AFPs to ice. This is consistent with computer simulations of methane hydrate growth showing that the interface between the liquid and hydrate crystal is ~10–20 Å thick and not well ordered (34), which is comparable with the ice-water interface (35,36).

Our model can also explain the curious hydrate binding behavior of the type I A17L mutant. It is well established that the A17L mutant is inactive in ice binding, and this has been previously explained by the presence of a bulky side chain projecting from the IBS that would sterically prevent binding to ice (37). However, this ice-inactive mutant is an even stronger inhibitor of hydrate binding than the wild-type protein (17). According to our hydrate-binding model (Fig. 6), Ala 17 (at the i+4 position) docks into the largest groove (groove 2) of the {100} planes. If this residue is substituted by Leu, the larger side chain would still fit snugly (Fig. 8). Therefore, the binding of the mutant to sII hydrate could potentially be more favorable.

Implications for the rational design of KHIs

The development of KHIs started in the late 1980s using trial and error (38). In the hopes of designing more effective inhibitors, several molecular modeling studies have been done to

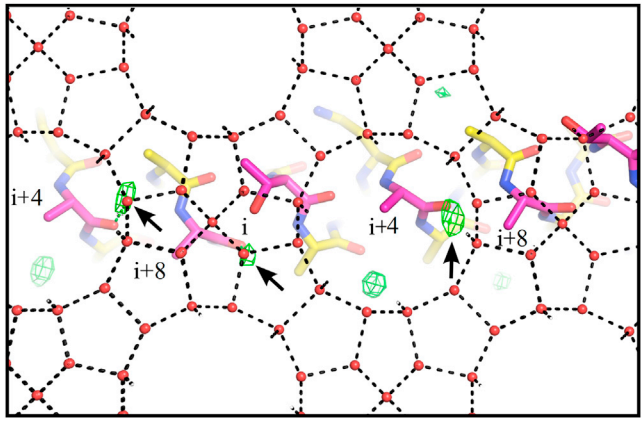

FIGURE 7 Type I AFP with the predicted surface waters docks to gas hydrate {100} planes. Type I AFP (*stick representation*) below the hydrate water surface is shown with carbon atoms (*yellow*), and ice-binding residues (purple) and their periodic positions labeled as in Fig. 6. The predicted water densities on the surface of type I AFP (*green mesh*) are shown with the contour level set to 0.9. Waters that are predicted to be anchored by the carbonyl groups of the ice-binding residues at positions i+4 and i+8 are indicated by arrows. The hydrate waters on the {100} planes (*red spheres*), and their hydrogen bonds (*black dashed lines*) are also indicated. To see this figure in color, go online.

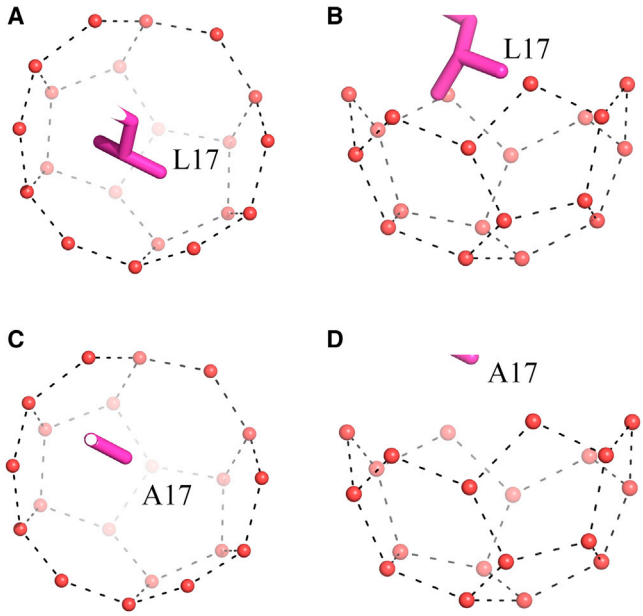

FIGURE 8 Accommodation of the Leu 17 side chain in a groove when type I AFP mutant docks to the {100} hydrate planes. (*A* and *B*) The side chain of Leu 17 (*purple stick representation*) is shown, with waters that form one groove 2 on the {100} planes (*red spheres*) and their hydrogen bonds (*black dashed lines*) also indicated. (*A*) Top view. (*B*) Side view. (*C* and *D*) As a comparison, the docking of Ala 17 in the same groove where the wild-type binds is also shown. (*C*) Top view. (*D*) Side view. To see this figure in color, go online.

elucidate the mechanism by which KHIs bind to gas hydrates (29–33,39). Although some experimental results supported these computational studies, it is not clear if the applied simulation methods, conditions, and parameters were accurate enough to reveal the interaction complexities. Here, we present detailed binding models for type I AFP and Maxi to sII hydrates based on crystallographic as well as experimental data. We think these models will help inspire the rational design of effective KHIs. First, the model of type I AFP bound to gas hydrate can serve as a standard to optimize computations, which can then be applied to other KHIs to assess their interactions with certain planes of the gas hydrate. Also, the binding mechanism proposed here based on our models suggests alternative strategies for designing KHIs. In each repeat, the amide group should anchor a water molecule that matches well with a hydrate plane; the hydrophobic group should project well into the cavities of the hydrate, as exemplified by Maxi, type I AFP, and its A17L mutant. In practice, these criteria can be achieved by changing the length of the repeat, the size of the hydrophobic group, and the distance between the amide and hydrophobic groups. In this manuscript, our key contribution to new KHI design is to consider how waters are organized on the inhibitor surface. The ACW binding mechanism proposed here based on our models suggests that a KHI may bind gas hydrates not directly but through its bound waters. This can be used to guide the rational design of hydrate inhibitors. The monomers of typical KHIs contain a vinyl group (used in polymerization) and a hydrate-binding site (containing amide and hydrophobic groups). We suggest that first, extensive MD simulations should be performed on a monomer of a potential KHI to reveal water organization around the hydrate-binding group. If these water patterns merge with sII, for example, the polymer or copolymer can then be designed to target specific hydrate plane(s). In the absence of complementation, the size of the hydrophobic group and the distance between the amide and hydrophobic groups can be varied until a match is obtained.

CONCLUSIONS

In summary, we have discovered that the internal water network of a novel AFP, Maxi, is remarkably similar to the {100} planes of sII gas hydrate. Since antifreeze proteins act as KHIs, these crystallographic data have facilitated the construction of in silico models for Maxi and type I AFP binding to sII hydrates, which were also corroborated by THF hydrate binding and previous experimental evidence. Both in silico and experimental data support the absorbance-inhibition mechanism proposed for KHI binding to gas hydrates. In addition, having the Maxi crystal structure with waters present has helped us suggest that the inhibitor binds to gas hydrate lattice through the anchored clathrate water mechanism. These detailed adsorption models will help inspire the rational design of a next generation of effective green KHIs for the petroleum industry to ensure safe and efficient hydrocarbon flow.

SUPPORTING MATERIAL

One figure is available at http://www.biophysj.org/biophysj/supplemental/S0006-3495(15)00923-6.

AUTHOR CONTRIBUTIONS

V.K.W. and P.L.D. designed the research; T.S. performed the research; and T.S., P.L.D., and V.K.W analyzed the data and wrote the manuscript.

ACKNOWLEDGMENTS

We gratefully acknowledge Kristy Moniz for technical help, Dr. Rob Campbell for advice on modeling, and the High Performance Computing Virtual Laboratory facility for computational time.

This work was supported by funds from Natural Sciences and Engineering Research Council of Canada to V.K.W. and from the Canadian Institutes of Health Research to P.L.D. T.S. holds an Ontario Graduate Scholarship, P.L.D. holds the Canada Research Chair in Protein Engineering, and V.K.W. holds a Queen's University Research Chair.

REFERENCES

1. Kvenvolden, K. A. 1993. Gas hydrates—geological perspective and global change. *Rev. Geophys.* 31:173–187.

2. Sloan, E. D., Jr. 2003. Fundamental principles and applications of natural gas hydrates. *Nature.* 426:353–363.
3. Walker, V. K., H. Zeng, …, P. Englezos. 2015. Antifreeze proteins as gas hydrate inhibitors. *Can. J. Chem.* 93:839–849.
4. Koh, C. A., R. E. Westacott, …, A. K. Soper. 2002. Mechanisms of gas hydrate formation and inhibition. *Fluid Phase Equilib.* 194–197:143–151.
5. McLaurin, G., K. Shin, …, J. A. Ripmeester. 2014. Antifreezes act as catalysts for methane hydrate formation from ice. *Angew. Chem. Int. Ed. Engl.* 53:10429–10433.
6. Lederhos, J. P., J. P. Long, …, E. D. Sloan, Jr. 1996. Effective kinetic inhibitors for natural gas hydrates. *Chem. Eng. Sci.* 51:1221–1229.
7. Huo, Z., E. Freer, …, E. D. Sloan, Jr. 2001. Hydrate plug prevention by anti-agglomeration. *Chem. Eng. Sci.* 56:4979–4991.
8. Marshall, C. B., G. L. Fletcher, and P. L. Davies. 2004. Hyperactive antifreeze protein in a fish. *Nature.* 429:153.
9. Marshall, C. B., A. Chakrabartty, and P. L. Davies. 2005. Hyperactive antifreeze protein from winter flounder is a very long rod-like dimer of α-helices. *J. Biol. Chem.* 280:17920–17929.
10. Nutt, D. R., and J. C. Smith. 2008. Dual function of the hydration layer around an antifreeze protein revealed by atomistic molecular dynamics simulations. *J. Am. Chem. Soc.* 130:13066–13073.
11. Meister, K., S. Strazdaite, …, H. J. Bakker. 2014. Observation of ice-like water layers at an aqueous protein surface. *Proc. Natl. Acad. Sci. USA.* 111:17732–17736.
12. Meister, K., S. Ebbinghaus, …, M. Havenith. 2013. Long-range protein-water dynamics in hyperactive insect antifreeze proteins. *Proc. Natl. Acad. Sci. USA.* 110:1617–1622.
13. Yang, C., and K. A. Sharp. 2004. The mechanism of the type III antifreeze protein action: a computational study. *Biophys. Chem.* 109:137–148.
14. Garnham, C. P., R. L. Campbell, and P. L. Davies. 2011. Anchored clathrate waters bind antifreeze proteins to ice. *Proc. Natl. Acad. Sci. USA.* 108:7363–7367.
15. Sun, T., F. H. Lin, …, P. L. Davies. 2014. An antifreeze protein folds with an interior network of more than 400 semi-clathrate waters. *Science.* 343:795–798.
16. Sharp, K. A. 2014. The remarkable hydration of the antifreeze protein Maxi: a computational study. *J Chem Phys.* 141:22D510.
17. Zeng, H., L. D. Wilson, …, J. A. Ripmeester. 2006. Effect of antifreeze proteins on the nucleation, growth, and the memory effect during tetrahydrofuran clathrate hydrate formation. *J. Am. Chem. Soc.* 128:2844–2850.
18. Daraboina, N., P. Linga, …, P. Englezos. 2011. Natural gas hydrate formation and decomposition in the presence of kinetic inhibitors. 2. Stirred reactor experiments. *Energy Fuels.* 25:4384–4391.
19. Gordienko, R., H. Ohno, …, V. K. Walker. 2010. Towards a green hydrate inhibitor: imaging antifreeze proteins on clathrates. *PLoS One.* 5:e8953.
20. 2002. The PyMOL Molecular Graphics System, Version 1.54. Schrödinger, LLC.
21. Van Der Spoel, D., E. Lindahl, …, H. J. Berendsen. 2005. GROMACS: fast, flexible, and free. *J. Comput. Chem.* 26:1701–1718.
22. Sharifi, H., V. K. Walker, …, P. Englezos. 2014. Inhibition activity of antifreeze proteins with natural gas hydrates in saline and the light crude oil mimic, heptane. *Energy Fuels.* 28:3712–3717.
23. Garnham, C. P., A. Natarajan, …, P. L. Davies. 2010. Compound ice-binding site of an antifreeze protein revealed by mutagenesis and fluorescent tagging. *Biochemistry.* 49:9063–9071.
24. Tavlarakis, P., J. J. Urban, and N. Snow. 2011. Determination of total polyvinylpyrrolidone (PVP) in ophthalmic solutions by size exclusion chromatography with ultraviolet-visible detection. *J. Chromatogr. Sci.* 49:457–462.
25. Yang, C., and K. A. Sharp. 2005. Hydrophobic tendency of polar group hydration as a major force in type I antifreeze protein recognition. *Proteins.* 59:266–274.
26. Kelland, M. A. 2009. Production Chemicals for the Oil and Gas Industry. Taylor and Francis Group, LLC, Boca Raton, FL, p. 213.
27. Hawtin, R., and P. M. Rodger. 2006. Polydiversity in oligomeric low dosage gas hydrate inhibitors. *J. Mater. Chem.* 16:1934–1942.
28. Aldiwan, N., Y. Lui, …, C. Koh. 2008. Neutron diffraction and EPSR simulations of the hydrate structure around propane molecules before and during gas hydrate formation. *Proc. Intl. Conf. Gas Hydrates, 6th, Vancouver, British Columbia, Canada*. 6–10.
29. Anderson, B. J., J. W. Tester, …, B. L. Trout. 2005. Properties of inhibitors of methane hydrate formation via molecular dynamics simulations. *J. Am. Chem. Soc.* 127:17852–17862.
30. Hawtin, R. W., D. Quigley, and P. M. Rodger. 2008. Gas hydrate nucleation and cage formation at a water/methane interface. *Phys. Chem. Chem. Phys.* 10:4853–4864.
31. Cruz-Torres, A., A. Romero-Martínez, and A. Galano. 2008. Computational study on the antifreeze glycoproteins as inhibitors of clathrate-hydrate formation. *ChemPhysChem.* 9:1630–1635.
32. Makogon, T. Y., R. Larsen, …, E. D. Sloan, Jr. 1997. Melt growth of tetrahydrofuran clathrate hydrate and its inhibition. *J. Cryst. Growth.* 179:258–262.
33. Wathen, B., P. Kwan, …, V. K. Walker. 2010. Modeling the interactions between poly(N-vinylpyrrolidone) and gas hydrates: factors involved in suppressing and accelerating hydrate growth. *Lect. Notes Comput. Sci.* 5976:117–133.
34. Vatamanu, J., and P. G. Kusalik. 2006. Molecular insights into the heterogeneous crystal growth of si methane hydrate. *J. Phys. Chem. B.* 110:15896–15904.
35. Gulam Razul, M. S., J. G. Hendry, and P. G. Kusalik. 2005. Mechanisms of heterogeneous crystal growth in atomic systems: insights from computer simulations. *J. Chem. Phys.* 123:204722.
36. Razul, M. S. G., E. V. Tam, …, P. G. Kusalik. 2005. Computer simulations of heterogeneous crystal growth of atomic systems. *Mol. Phys.* 103:1929–1943.
37. Baardsnes, J., L. H. Kondejewski, …, P. L. Davies. 1999. New ice-binding face for type I antifreeze protein. *FEBS Lett.* 463:87–91.
38. Kelland, M. A. 2006. History of the development of low dosage hydrate inhibitors. *Energy Fuels.* 20:825–847.
39. Bagherzadeh, S. A., S. Alavi, …, P. Englezos. 2015. Why ice-binding type I antifreeze protein acts as a gas hydrate crystal inhibitor. *Phys. Chem. Chem. Phys.* 17:9984–9990.

Supplemental Material

Structural Basis for the Inhibition of Gas Hydrates by Alpha-helical Antifreeze Proteins

Tianjun Sun[†], Peter L. Davies [†,‡] and Virginia K. Walker *[†,‡]

[†]Department of Biomedical and Molecular Sciences, Queen's University, Kingston, Ontario, Canada

[‡]Department of Biology, Queen's University, Kingston, Ontario, Canada

Figure S1. The polycrystalline THF crystal grown in the presence of 4 μM PVP.